Energy 36 (2011) 6208–6219

Contents lists available at ScienceDirect

Energy

journal homepage: www.elsevier.com/locate/energy

Comparison of trilateral cycles and organic Rankine cycles

Johann Fischer*

Institut für Verfahrens- und Energietechnik, Universität für Bodenkultur, Muthgasse 107, A-1190 Wien, Austria

ARTICLE INFO

Article history:
Received 6 April 2011
Received in revised form
27 June 2011
Accepted 24 July 2011
Available online 31 August 2011

Keywords:
Heat to power conversion
Trilateral cycle
Organic Rankine cycle
Process optimization
Exergy analysis

ABSTRACT

A comparison of optimized trilateral cycle (TLC) - systems with water as working fluid and optimized organic Rankine cycle (ORC) – systems with pure organic working fluids is presented. The study includes the heat transfer to and from the cycles. The TLC - systems were optimized by the selection of the maximum water temperature, the ORC - systems by the selection of the working fluid and the process parameters. The optimization criterion is the exergy efficiency for power production being the ratio of the net power output to the incoming exergy flow of the heat carrier. Results will be presented for five different cases specified by the inlet temperature of the heat carrier and the inlet temperature of the cooling agent. The inlet temperature pairs are (350 °C, 62 °C), (280 °C, 62 °C), (280 °C, 15 °C), (220 °C, 15 °C) and (150 °C, 15 °C). It is found that the exergy efficiency for power production is larger by 14%–29% for the TLC than for the ORC. On the other hand, the outgoing volume flows from the expander are larger for the TLC than for the ORC by a factor ranging from 2.8 for the first case to 70 for the last case.

1. Introduction

Conversion of heat to power is a long-standing challenge for which the basic physical principles have already been worked out in the 19th century by Carnot [1], Clausius [2] and Rankine [3]. Presently, there is rapidly increasing interest in technologies for conversion of heat with low and moderate temperatures which is available e.g. as solar, geothermal, biogenic or waste heat. For conversion of this heat to power one can consider Clausius–Rankine cycles with organic working fluids called organic Rankine cycles (ORC) [4–30], Kalina cycles [28–36], and trilateral cycles (TLC) [37–44]; in view of the large number of publications about these cycles the references given are by far not complete. Whilst ORC and Kalina processes are used already in existing power plants, the TLC are still in a state of technical development and less known.

As TLC are less similar to Carnot cycles [1] than Clausius–Rankine cycles one expects TLC to have a smaller thermal efficiency than ORC at the same maximum and minimum cycle temperatures. The advantage of the TLC, however, is the more efficient heat transfer from the heat carrier to the working fluid of the cycle. Hence, in order to come to a practically relevant comparison of ORC and TLC one has to perform model calculations for systems which include the heat transfer from the heat carrier to the working fluid, the cycle process, and the heat transfer from the working fluid to the cooling agent. For comparisons of the systems efficiencies the inlet temperatures of the heat carrier and of the cooling agent have to be the same for the TLC- and the ORC-systems.

It was estimated by Löffler [40] that TLC - systems have efficiencies which are 50%–100% higher than those of ORC - systems. Model calculations for comparison of TLC - and ORC - systems have been published by Zamfirescu and Dincer [43]. They considered a heat carrier inlet temperature of 150 °C and a cooling air temperature of 25 °C. The TLC working fluids were ammonia + water mixtures and the ORC working fluids were pure R141b, R123, R245ca, and R21. They found that the exergy efficiency for power production ξ_P being the ratio of the net power output to the incoming exergy flow of the heat carrier is about 2–3 times larger for the TLC than for the ORC. In the estimates of Löffler [40] and in the calculations of Zamfirescu and Dincer [43], however, rather low values for the maximum ORC pressures have been selected; from Fig. 7 in [43] we conclude that the maximum pressure of R21 was about 1.47 MPa which is only 28% of the critical pressure. On the other hand, it is known [24,45] that the power output of ORC systems can be remarkably increased by using higher pressures which are slightly subcritical or supercritical. For such pressures the isobar of the working fluid during heating matches much better the isobar of the heat carrier. Hence, a comparison of higher pressure ORC with TLC remains a challenging task.

In this paper we will consider optimized TLC-systems with water as working fluid and optimized ORC systems with pure organic

* Tel.: +43 1 3709726 201; fax: +43 1 3709726 210.
E-mail address: johann.fischer@boku.ac.at.

0360-5442/$ – see front matter © 2011 Elsevier Ltd. All rights reserved.
doi:10.1016/j.energy.2011.07.041

Nomenclature

CHP	combined heat power
$\dot{C}$	heat capacity flow rate [kW/K]
c_p	heat capacity of the heat carrier [kJ/kgK]
e	specific exergy [kJ/kg]
$\dot{E}$	exergy flow rate [kW]
h	specific enthalpy [kJ/kg]
$\dot{H}$	enthalpy flow rate
IHE	internal heat exchanger
$\dot{m}$	mass flow rate [kg/s]
o2	ORC cycle at subcritical p_{max} without superheating
o3	ORC cycle at subcritical p_{max} with superheating
ORC	Organic Rankine cycle
p	pressure [MPa]
q	specific heat [kJ/kg]
$\dot{Q}$	heat flow rate [kW]
s	specific entropy [kJ/kgK] or [J/molK]
s2	ORC cycle at supercritical p_{max}
T	temperature [K] or [°C]
TLC	trilateral cycle
v	specific volume [l/kg][1]
$\dot{V}$	volume flow rate [l/s][1]
w	specific work [kJ/kg]
$\lvert\dot{W}\rvert$	net power output of a cycle [kW]

Greek symbols

Δ	difference of quantities
$\Delta\dot{H}$	enthalpy flow rate transferred to the working fluid [kW]
$\eta_{s,P}$	isentropic pump efficiency
$\eta_{s,T}$	isentropic turbine efficiency
η_{th}	thermal efficiency of the cycle
ξ	total exergy efficiency
ξ_P	exergy efficiency for power production

Subscripts

1,2,3,4,	state points of working fluid in TLC and ORC
2a,4a	state points of working fluid in ORC with IHE
5,6	state points of heat carrier
7,8	state points of cooling agent
c	critical point
i	state point
ij	process from state point i to j
in	ingoing flow; Inlet temperature
max	maximum quantities of working fluid (state point 3)
min	minimum quantities of working fluid (state point 1)
out	Outgoing flow; Outlet temperature
P	Pump, Power
p	pinch (hot stream)
s	isentropic
T	turbine
u	environment state
WF	working fluid
HC	heat carrier
CA	cooling agent

[1] $1l = 1 \times 10^{-3}$ m^3.

working fluids. The heat source temperatures range from 150 °C to 350 °C. Whilst the optimization of the TLC-systems concerns only the selection of the maximum water temperature, the ORC - systems are optimized with respect to the working fluid and the process parameters. For ORC-systems model calculations have been made for rather high heat source temperatures by Angelino and Colonna [8,9] and for rather low heat source temperatures by Lakew and Bolland [23]. For the temperature range considered here optimized model results with pure organic fluids were presented recently by Lai et al. [24] for ORC-systems including the heat transfer from the heat carrier to the working fluid.

Optimized model results will be presented for complete TLC- and ORC-systems for five different cases, which are specified by the inlet temperature of the heat carrier and the inlet temperature of the cooling agent. The inlet temperature pairs are for case I (350 °C, 62 °C), for case II (280 °C, 62 °C), for case III (280 °C, 15 °C), for case IV (220 °C, 15 °C) and for case V(150 °C, 15 °C). For the ORC we selected the best working fluids and the best process parameters on the basis of our previous study [24]. For all cases the optimization criterion was to find for a net power output of 1 MW the minimum heat capacity flow rate of the heat carrier $\dot{C}_{HC}$ This criterion corresponds to finding a maximum net power output for an available heat carrier with given temperature and heat capacity flow rate.

For comparison of the TLC- and the ORC-systems we use two measures. The first is the exergy efficiency for power production ξ_p [24] which is linear proportional to $1/\dot{C}_{HC}$ Hence, this measure corresponds to the applied optimization criterion. Now one may argue that ξ_p does not fully reflect the situation as in particular for higher inlet temperatures of the cooling agent the outgoing flows of the heat carrier and of the cooling agent contain still remarkable exergy flows which could still be used e.g. in cascade systems or in combined heat power (CHP) plants. Hence, we use as second measure the total exergy efficiency ξ which is the ratio of all outgoing exergy flows to all incoming exergy flows of the system.

The paper is organized such that in Sec. 2 the TLC- system is described. As the TLC- process is not so well known we explain also the "ideal" TLC-process. In Sec. 3 the ORC-system is described shortly as it has been treated previously already in detail in Ref. [11,24]. In Sec. 4 the supply of the heat to the cycles and its removal are considered together with a full exergetic analysis of the systems. In Sec. 5 we consider the five cases mentioned above,

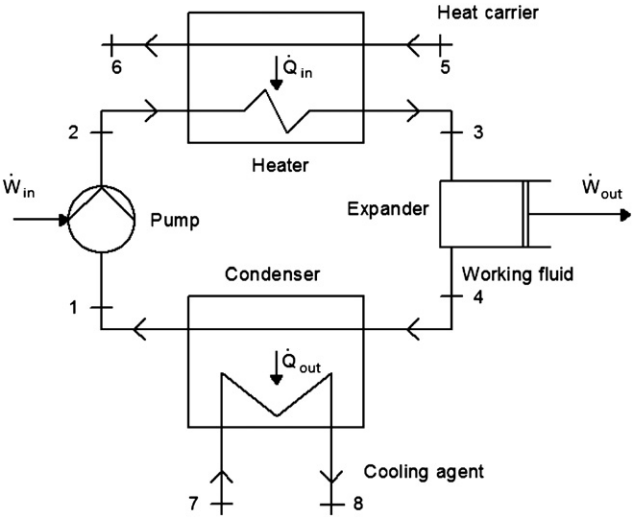

Fig. 1. Configuration of a TLC- system.

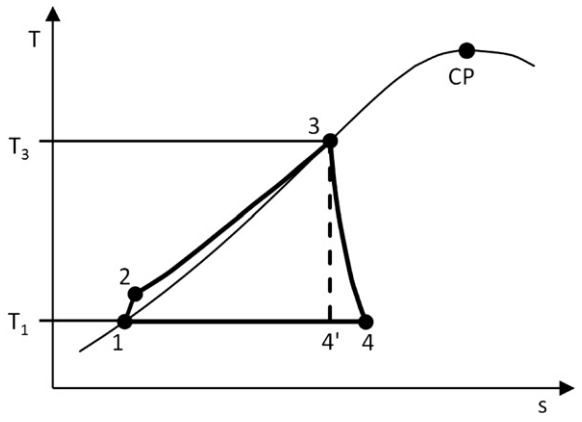

Fig. 2. The Trilateral cycle in the T,s-diagram.

discuss the selection of the working fluids and the cycle types of the ORC-systems and present the optimized results for the TLC- and ORC- systems. Finally, in Sec. 6 a general discussion and conclusions will be given.

2. Description of the trilateral cycle

2.1. Configuration of the TLC-system

The TLC-system is shown in Fig. 1 and consists of the trilateral cycle to which heat is supplied from the heat carrier and removed by the cooling agent.

The TLC-plant consists of a pump, a heater, a two-phase expander and a condenser. In state 1 the working fluid is saturated liquid water with temperature T_1 at the vapour pressure p_1. Then the pressure of the liquid is increased by the pump to p_2 at state 2 in the homogeneous liquid. Thereafter, the liquid water

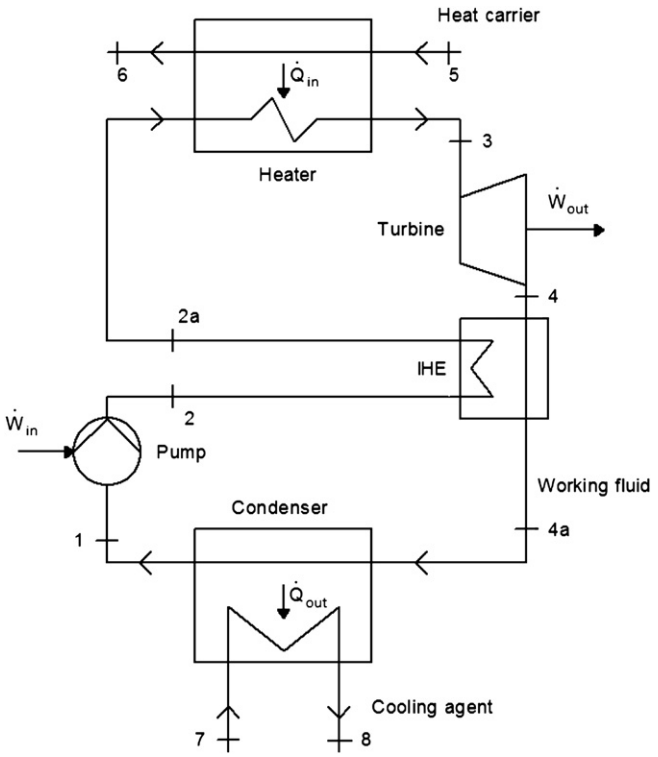

Fig. 3. Configuration of an ORC- system with internal heat exchanger (IHE).

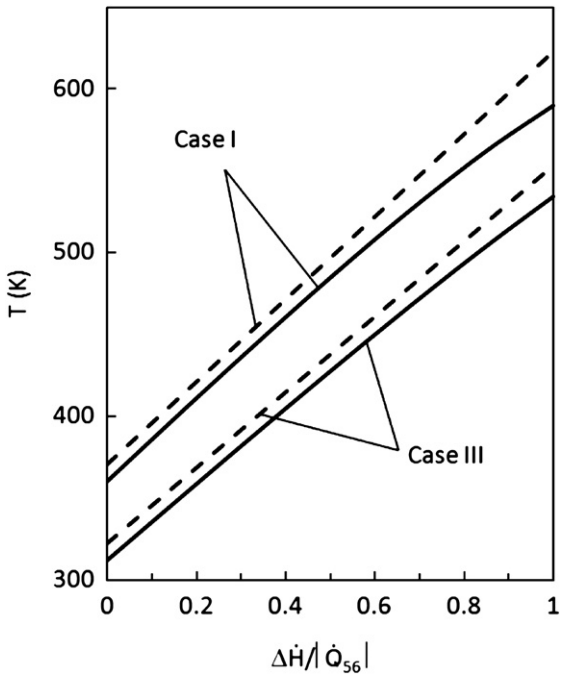

Fig. 4. T, $\Delta\dot{H}$ -diagram for the heat transfer from the heat carrier to the working fluid in the TLC-systems for cases I and III. - - - - heat carrier, —— working fluid.

enters the heater where it is heated up just to its boiling point at pressure p_2 which is state 3. The temperature T_3 is the boiling temperature at pressure p_2. At state 3 the fluid enters the two-phase expander. In the expander the liquid expands into the wet vapour region down to pressure p_1 and arrives at state 4 with temperature T_1 and vapour content x. During this process step the working fluid delivers work. Finally, starting from state 4 the wet vapour is completely condensed till it reaches state 1.

As already mentioned, the heat is supplied to the TLC-plant from a heat carrier which enters the heater at temperature T_5

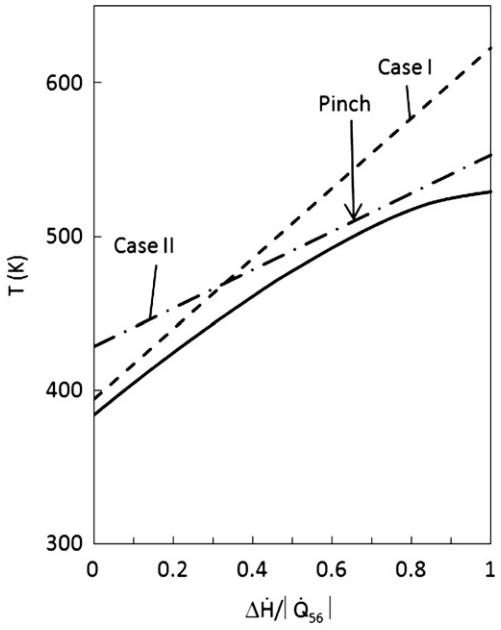

Fig. 5. T, $\Delta\dot{H}$ -diagram for the heat transfer from the heat carrier to the working fluid in the ORC-s2 -systems for cases I and II. - - - - heat carrier for case I, —•—•—• heat carrier for case II, —— working fluid. For case I the pinch is at the cold end of the heat carrier, for case II the pinch is indicated in the figure.

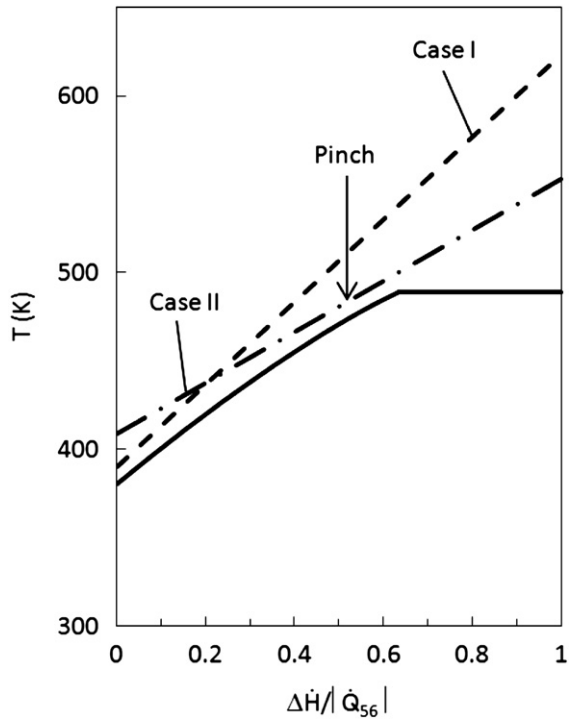

Fig. 6. T, ΔḢ -diagram for the heat transfer from the heat carrier to the working fluid in the ORC-o2 -systems for cases I and II. - - - - heat carrier for case I, –• –• –• – heat carrier for case II, —— working fluid. For case I the pinch is at the cold end of the heat carrier, for case II the pinch is indicated in the figure.

and leaves it at temperature T_6. The heat is removed by a cooling agent which enters the condenser at temperature T_7 and leaves it at temperature T_8.

The two-phase expander is the technically most challenging component and may be a turbine, a scroll expander, a screw expander or a reciprocating engine. Recent developments are described for a screw-type engine in [39] and for a reciprocating engine in [40,42,44].

2.2. Thermodynamics of the TLC-process

A schematic representation of the TLC in a temperature vs entropy (T,s)-diagram is shown in Fig. 2, where CP is the critical point of the working fluid and the curve connecting points 1, 3, and CP is the boiling curve. In the following, the quantities T_i, p_i, h_i, s_i and v_i denote the temperature, the pressure, the specific enthalpy, the specific entropy and the specific volume at state point i and the quantities w_{ij} and q_{ij} denote the specific work and heat in the process from state point i to state point j.

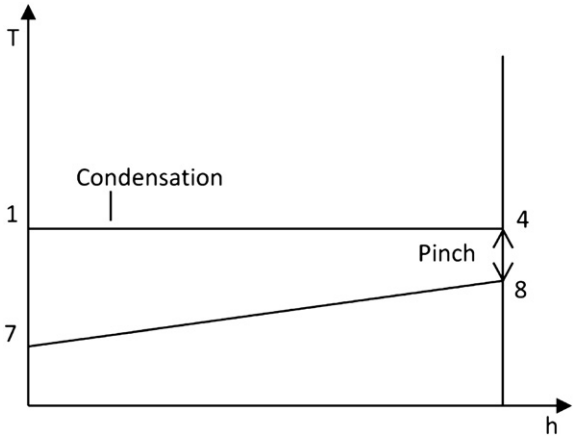

Fig. 7. T,h-diagram for the heat transfer from the working fluid to the cooling agent in the TLC- systems.

At state point 1 the working fluid is saturated liquid water at T_1 and the corresponding vapour pressure p_1 where $T_1 = T_{min}$ is the minimum temperature and $p_1 = p_{min}$ is the minimum pressure in the TLC. By adiabatic compression to p_2 which is the maximum pressure in the TLC, $p_2 = p_{max}$, the state point 2 is reached in the homogeneous liquid at temperature T_2. The specific work w_{12} required for compression with an isentropic pump efficiency $\eta_{sP} = (h_{2'} - h_1)/(h_2 - h_1)$ is $w_{12} = h_2 - h_1$. The hypothetical state point 2′ (not shown in Fig. 2) lies on the isobar p_2 and has the same entropy as state 1, $s_{2'} = s_1$. From point 2 the liquid flows isobarically through the heater till it arrives at its boiling temperature at point 3. The temperature T_3 is the maximum temperature T_{max} in the TLC, $T_3 = T_{max}$. During that process the working fluid takes up the specific heat $q_{23} = h_3 - h_2$. At point 3 the working fluid enters the expander where it undergoes a flash expansion till it arrives at point 4 in the wet vapour region with pressure p_1, temperature T_1 and vapour content x. During that expansion the specific work $w_{34} = h_4 - h_3$ is delivered from the expander with the isentropic expander efficiency $\eta_{sE} = (h_4 - h_3)/(h_{4'} - h_3)$. The hypothetical state point 4′ shown in Fig. 2 lies on the isobar p_1 and has the same entropy as state 3, $s_{4'} = s_3$. At state point 4 the working fluid enters the condenser in which it returns isobarically to state point 1 by releasing the specific heat $q_{41} = h_4 - h_1$ to the cooling agent.

Summarizing, for the TLC the net specific work is $w = w_{12} + w_{34}$ and the supplied specific heat is q_{23}. Then the thermal efficiency η_{th} of the cycle is

$$\eta_{th} = |w_{12} + w_{34}|/q_{23}, \tag{1}$$

and for a mass flow rate of the working fluid $\dot{m}_{WF}$ the net power output is

$$|\dot{W}| = \dot{m}_{WF}|w_{12} + w_{34}|. \tag{2}$$

Finally, the volume flow rate at a given state with specific volume v is given by

$$\dot{V} = \dot{m}_{WF}\ v. \tag{3}$$

The thermodynamics of the supply of heat to the cycle and its removal from the cycle will be considered in Sec. 4 for the TLC- and the ORC-system.

2.3. The ideal TLC

The concept of the ideal TLC is described already in the literature [37,40]. But as these sources are difficult to access the ideal TLC is explained here again shortly for convenience of the reader by using Fig. 2. As state point 2 is very close to state point 1 in a T,s-diagram it is assumed in the ideal TLC that point 2 coincides with point 1 in the T,s-diagram. Then one moves along an isobar from 1 to 3. Thereafter, the flash expansion from 3 to 4 is assumed to be isentropic so that point 4 coincides with 4′. Hence, the ideal TLC is represented by the isobar from 1 = 2 to 3, the vertical isentrope from 3 to 4 and the horizontal isotherm from 4 to 1.

For deriving the equation of the isobar in the T,s-diagram, we start from the thermodynamic relation

$$dh = Tds + vdp, \tag{4}$$

which for an isobar simplifies to $dh = Tds$. Moreover using the isobaric relation $dh = c_p dT$ one obtains

$$ds = (c_p/T)dT, \tag{5}$$

which, assuming constant c_p, can be integrated to yield

$$s - s_1 = c_p \ln(T/T_1), \tag{6}$$

or

$$T = T_1 \exp[(s - s_1)/c_p]. \tag{7}$$

Next, the heat transferred to ideal TLC along the isobar from 1 = 2 to 3 is simply

$$q_{23} = c_p(T_3 - T_1), \tag{8}$$

whilst the heat removed from the ideal TLC along the isotherm from 4 to 1 is given by the area (with negative sign) below that isotherm in the T,s-diagram

$$q_{41} = -T_1(s_4 - s_1) = -T_1(s_3 - s_1), \tag{9}$$

which can be written by using Eq. (6) as

$$q_{41} = -c_p T_1 \ln(T_3/T_1). \tag{10}$$

Ignoring the small work for compression from 1 to 2, the first law requires that

$$w_{34} = -q_{23} - q_{41}, \tag{11}$$

which by insertion of (8) and (9) yields the work

$$w_{34} = -c_p(T_3 - T_1) + c_p T_1 \ln(T_3/T_1), \tag{12}$$

and there from the thermal efficiency $\eta_{th} = -w_{34}/q_{23}$ of an ideal TLC is obtained as

$$\eta_{th} = 1 - \ln(T_3/T_1)/[(T_3/T_1) - 1]. \tag{13}$$

Some authors [41] replace the exponential isobar from 1 = 2 to 3 in the T,s-diagram by a straight line, which then yields the thermal efficiency η_{th} as

$$\eta_{th} = (T_3 - T_1)/(T_1 + T_3) \tag{14}$$

3. Description of the organic Rankine cycle

3.1. Configuration of the ORC- system

The plant configuration of an ORC-system with internal heat exchanger (IHE) is shown in Fig. 3. The IHE transfers heat from (4,4a) to (2,2a) and is not contained in the most simple configuration. The ORC-system shown in Fig. 3 includes also the heat supply and removal.

The plant without IHE consists of a pump, a heater, a turbine and a cooler-condenser. In state 1 the working fluid is a saturated liquid with temperature T_1 at the pressure p_1, where $T_1 = T_{min}$ is the minimum temperature and $p_1 = p_{min}$ is the minimum pressure in the cycle. Then the pressure of the liquid is increased by the pump with isentropic pump efficiency η_{sP} to $p_2 = p_{max}$, which is the maximum pressure in the cycle. Thereafter, the fluid is heated in an isobaric process to the temperature $T_3 = T_{max}$ which is the maximum temperature in the cycle. In case that p_{max} is lower than the critical pressure p_c of the working fluid, the process step from 2 to 3 includes heating of the liquid to saturation, evaporation of the liquid and eventually superheating of the vapour. In case that p_{max} is higher than p_c, there is no phase transition in going from 2 to 3 and the fluid in state 3 is supercritical. At state point 3 the fluid enters the turbine where it expands with isentropic expander efficiency η_{sE} to the pressure p_{min} at state 4 and delivers work in this process step. Finally, starting from state 4 the fluid is first cooled to the temperature T_{min} and then condensed in an isobaric process till it reaches state 1.

It is known e.g. from [11,24] that for many cycles the temperature at state 4 after the turbine is considerably higher than at state 1. Hence it may be rewarding to implement an IHE for heat recovery within the cycle. The low pressure vapour cools down from state 4 to 4a and the heat is transferred to the compressed liquid which is heated up from state 2 to state 2a.

The heat supply in the heater and its removal in the cooler-condenser are also shown in Fig. 3 and are similar to those in the TLC-system.

3.2. Thermodynamics of the ORC process

ORC-processes have a greater variety than TLC—processes [11,24]. With respect to the maximum pressure they can either be subcritical or supercritical (*s*), the shape of the coexistence curve can either be bell-shaped (*b*) or overhanging (*o*) and in subcritical cycles state 3 can either be on the dew line or in the superheated vapour. Moreover, the cycle can be run with or without IHE. For clarity, we have introduced in [11] a nomenclature which distinguishes subcritical cycles b1, b2, b3 for bell-shaped T,s-diagrams, subcritical cycles o2, o3 for overhanging T,s-diagrams, and supercritical cycles s1, s2. Here, we will consider only s2 and o2 cycles, for which T,s- diagrams are shown in Figs. 2 and 4 of [24].

From the T,s-diagrams in Figs. 2 and 4 of [24] it can be seen that for the cycles s2 and o2 the temperature T_4 at state 4 can be remarkably higher than the temperature T_1 of the condenser. Hence it is rewarding to use an IHE in which the hot stream is cooled down from T_4 to T_{4a} which has to be higher than T_2; we call $T_{4a} - T_2 = \Delta T_{IHE}$. The enthalpy difference $h_4 - h_{4a}$ is transferred adiabatically to the cold stream which is heated up from T_2 to T_{2a} with an enthalpy difference $h_{2a} - h_2 = h_4 - h_{4a}$.

In the cycles without IHE the heat $q_{23} = h_3 - h_2$ is added to the working fluid during the process (2-3) and the heat q_{41} is removed from it during the process (4–1). The work w_{34} is taken from the turbine during the process (3–4) and a small amount of work w_{12} is required to pump the liquid during the process (1–2). For the heat q_{41} and the works w_{12} and w_{34} the same equations hold for the ORC as for the TLC. Hence, the thermal efficiency of a cycle without IHE is given again by Eq. (1) whilst for a cycle with IHE only the heat q_{2a3} has to be added to the working fluid and hence the thermal efficiency is given in these cases as

$$\eta_{th} = |w_{12} + w_{34}|/q_{2a3}(\text{ORC with IHE}). \tag{15}$$

For a mass flow rate of the working fluid $\dot{m}_{WF}$ the net power output is given by Eq. (2) and the volume flow rate by Eq. (3).

4. The TLC- and the ORC- systems with supply and removal of the heat

As already mentioned in the Introduction the efficiency of the heat to power conversion systems does not only depend on the thermal efficiency of the cycle but also substantially on the heat transfer to the cycle and to minor extent also on the heat removal from the cycle. For the operation of such a system, one usually has a heat carrier available with a given inlet temperature T_5, a mass flow rate $\dot{m}_{HC}$ and a heat capacity $c_{p,HC}$. It is convenient to combine the two latter quantities to the heat capacity flow rate $\dot{C}_{HC} = c_{p,HC}\dot{m}_{HC}$. On the cold end one has a cooling agent with inlet temperature T_7 which may either be close to the environmental temperature or remarkably higher in case that the removed heat is still used, e.g. in district heating or a cascade process. The required

mass flow $\dot{m}_{CA}$ of the cooling agent or its hho;eat capacity flow rate $\dot{C}_{CA} = c_{\rho,CA} \cdot \dot{m}_{CA}$ will result from the design of the whole system.

The remaining question is that for the objective function to which the system shall be optimized. For sure, a minimization of the exergy loss may be of interest but from a practical point of view one might be more interested in maximizing the net power output $|\dot{W}|$. For convenience of comparison we decided here as already in [24] to assume a given net power output $|\dot{W}|$ of 1 MW and to take as objective function the minimum of the heat capacity flow rate $\dot{C}_{HC}$ of the heat carrier. To summarize, the boundary conditions of the system are T_5, T_7 and the net power output $|\dot{W}| = 1$MW whilst the objective function for minimization is the heat capacity flow rate $\dot{C}_{HC}$ of the heat carrier.

The items at issue are now the heat transfers in the heater and the cooler-condenser. These heat transfers shall be considered by pinch analyses using $T, \Delta\dot{H}$ -diagrams.

Throughout this paper we assume that the heat carrier and the cooling agent flow through the heat exchangers with constant pressure and that their isobaric heat capacities $c_{p,HC}$ and $c_{p,CA}$ are constant. By these assumptions one obtains for the heat carrier and the cooling agent linear relationships for the temperature T as function of the enthalpy flow rate $\Delta\dot{H}$.

In the actual calculations we start for a selected working fluid and cycle type with given values of T_5 and T_7. Moreover, we couple throughout this paper T_1 to T_7 by $T_1 = T_7 + 23$ K and start with a trial-and-error temperature T_3. With these values of T_1 and T_3 the thermodynamic calculations of the working fluid cycle are performed which yield w_{12}, q_{23} or q_{2a3}, w_{34}, and q_{41} or q_{4a1}. Then the mass flow rate $\dot{m}_{WF}$ is determined by the requirement that the net power output $|\dot{W}| = \dot{m}_{WF}|w_{12} + w_{34}|$ is just 1 MW. Knowing $\dot{m}_{WF}$ allows the calculation of the heat flow rates $\dot{Q}_{23}$ for TLC or $\dot{Q}_{2a3}$ for ORC which have positive signs and of $\dot{Q}_{41}$ for TLC or $\dot{Q}_{4a1}$ for ORC which have negative signs by $\dot{Q}_{ij} = \dot{m}_{WF} q_{ij}$ As the heat exchangers are assumed as adiabatic these quantities yield immediately the heat flow rates $\dot{Q}_{56}$ (negative) and $\dot{Q}_{78}$ (positive) as $\dot{Q}_{56} = -\dot{Q}_{23}$ for TLC or $\dot{Q}_{56} = -\dot{Q}_{2a3}$for ORC and $\dot{Q}_{78} = -\dot{Q}_{41}$ or $\dot{Q}_{78} = -\dot{Q}_{4a1}$ for TLC or ORC resp. In subsequent steps one has to account for the heat transfer to the working fluid which is explained below.

4. 1. Heat transfer to the working fluid

In the heater the heat flow rate $|\dot{Q}_{56}|$ has to be transferred which is given by

$$|\dot{Q}_{56}| = \dot{m}_{HC}\, c_{p,HC}(T_5 - T_6) = \dot{C}_{HC}(T_5 - T_6), \tag{16}$$

wherein T_6 and $\dot{C}_{HC}$ are still to be determined. From Eq. (16) it is clear that for given $|\dot{Q}_{56}|$ the value of $\dot{C}_{HC}$ decreases with decreasing T_6. This is also intuitively clear as with increasing cooling of the heat carrier more heat can be transferred to the working fluid. The cooling of the heat carrier, however, is limited by the occurrence of a pinch point between the heat carrier and the working fluid, which has now to be found. First one has to determine the T vs h function for the working fluid in the heater, i.e. for the process from 2 or 2a to 3. There from the enthalpy flow rate $\Delta\dot{H} = \dot{m}_{WF} \cdot (h - h_2)$ or $\Delta\dot{H} = \dot{m}_{WF} \cdot (h - h_{2a})$ and hence also the T vs $\Delta\dot{H}$ function of the cold stream can be determined. Such curves have already been shown in Fig. 8 –10 of [11]. Next, the T vs $\Delta\dot{H}$ function of the hot stream, i.e. of the heat carrier, has to be considered which can be obtained from $\Delta\dot{H} = |\dot{Q}_{56}| + \dot{C}_{HC} \cdot (T - T_5)$ as

$$T = T_5 + \left(|\dot{Q}_{56}|/\dot{C}_{HC}\right)\left(\Delta\dot{H}/|\dot{Q}_{56}| - 1\right) \tag{17}$$

with the still unknown value of $\dot{C}_{HC}$ which determines the slope of this straight line. The next task is then to find the pinch point by

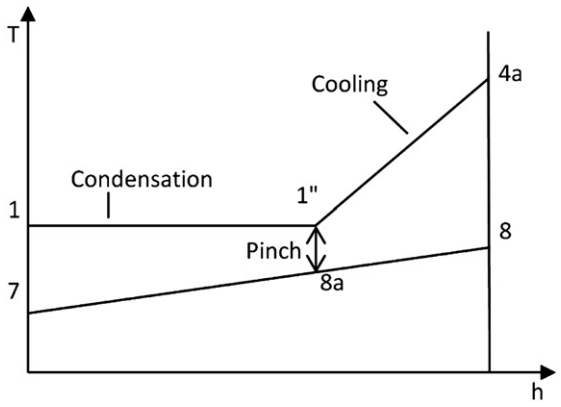

Fig. 8. T,h-diagram for the heat transfer from the working fluid to the cooling agent in the ORC – systems.

variation of the slope of the straight line till the minimum difference between the hot and cold stream curve ΔT_p becomes just equal to a prescribed value which is assumed to be 10 K. The temperature of the hot stream at that pinch point (or the upper pinch point temperature) is denoted by T_p. The largest possible slope $|\dot{Q}_{56}|/\dot{C}_{HC}$ of Eq.(17) determines then the minimum heat capacity flow rate $\dot{C}_{HC}$ of the heat carrier.

As the procedure was started for a selected working fluid and a selected cycle type and a trial-and-error temperature T_3 for given values of (T_5, T_7) one has to vary now first the temperature T_3 again with the objective to find a minimum value of $\dot{C}_{HC}$. In the ORC-systems one has thereafter still to screen different cycle types and working fluids.

Finally, we want to point out that the net power is given as $|\dot{W}| = |\dot{Q}_{56}|\eta_{th}$ or by use of Eq. (16) as

$$|\dot{W}| = \dot{C}_{HC}(T_5 - T_6)\eta_{th}, \tag{18}$$

which means that for a given net power output $|\dot{W}|$ of 1 MW the minimum of $\dot{C}_{HC}$ is obtained by the maximum of the product $(T_5 - T_6)\,\eta_{th}$. We remind that the thermal efficiency of the cycle is essentially determined by the maximum cycle temperature T_3 which can be achieved in the process. Concluding, the heat capacity flow rate $\dot{C}_{HC}$ can be minimized by a low value of T_6 and a high value of T_3.

4.1.1. Heat transfer to the working fluid in the TLC

Fig. 4 shows the T, $\Delta\dot{H}$ -diagram for the heat transfer from the heat carrier to the working fluid in the TLC-systems for Case I ($T_5 = 623.15$ K, $T_7 = 335.15$ K, $T_1 = 358.15$ K) and Case III ($T_5 = 553.15$ K, $T_7 = 288.15$ K, $T_1 = 311.15$ K). In that Figure as well as in the subsequent Figs. 5 and 6 the enthalpy flow rate $\Delta\dot{H}$ is reduced by $|\dot{Q}_{56}|$ to obtain a scale from 0 to 1. The dashed lines refer to the heat carrier, the full lines to the working fluid.

For Case I the heat carrier line ranges from $T_6 = 370.53$ K to $T_5 = 623.15$ K with the upper pinch point temperature being at $T_p = 416.16$ K, whilst the working fluid water with pressure $p_2 = 10.821$ MPa is heated from $T_2 = 360.20$ K to the boiling point temperature $T_3 = 590.00$ K. Hence, the temperature difference between the heat carrier and the working fluid amounts at the cold end to $T_6 - T_2 = 10.33$ K, decreases at the pinch point to $\Delta T_p = 10$ K and increases at the hot end to $T_5 - T_3 = 33.15$ K.

For Case III the heat carrier line ranges from $T_6 = 322.39$ K to $T_5 = 553.15$ K with the upper pinch point temperature being at $T_p = 388.53$ K, whilst the working fluid water with pressure $p_2 = 4.7574$ MPa is heated from $T_2 = 311.90$ K to the boiling point temperature $T_3 = 534.00$ K. Hence, the temperature difference

between the heat carrier and the working fluid amounts at the cold end to $T_6 - T_2 = 10.49$ K, decreases at the pinch point to $\Delta T_p = 10$ K and increases at the hot end to $T_5 - T_3 = 19.15$ K.

We observe from the Fig. 4 that the water isobars are in essence straight lines which become slightly curved downwards at higher temperatures. Because of this curvature the heat carrier and the working fluid curves are not strictly parallel and the temperature gap is larger at the hot end than at the cold end. Moreover, this curvature is the reason why the pinch point does not occur between states 2 and 6 but at some higher temperature.

With regard to the minimization of the heat capacity flow rate $\dot{C}_{HC}$ according to Eq. (18) we note that the temperatures T_6 are very low and only a few tenth of K above their limiting value $T_2 + \Delta T_p$. Moreover, the maximum cycle temperatures T_3 are also rather high and not very far below the heat carrier inlet temperature T_5. Both these facts are very favorable for low $\dot{C}_{HC}$ -values, which will be presented in Sec. 5.

4.1.2. Heat transfer to the working fluid in the ORC

Fig. 5 shows the T, $\Delta\dot{H}$ -diagram for the heat transfer from the heat carrier to the working fluid cyclopentane in the ORC-s2 -systems for case I ($T_5 = 623.15$ K, $T_7 = 335.15$ K, $T_1 = 358.15$ K) and Case II ($T_5 = 553.15$ K, $T_7 = 335.15$ K, $T_1 = 358.15$ K). The dashed line refers to the heat carrier for Case I, the dashed-dotted line refers to the heat carrier for Case II, and the full line refers to cyclopentane at the supercritical pressure $p_2 = 5.412$ MPa. First, we observe from Fig. 5 that the supercritical isobar of cyclopentane has a strong curvature in particular at higher temperatures.

For the ORC-s2 -system in Case I the heat carrier line ranges from $T_6 = 394.29$ K to $T_5 = 623.15$ K with the upper pinch point temperature being at the cold end, i.e. $T_p = T_6 = 394.29$ K, whilst the working fluid cyclopentane is heated from $T_{2a} = 384.29$ K to the temperature $T_3 = 529.00$ K. Hence, the temperature difference between the heat carrier and the working fluid amounts at the cold end with the pinch point $\Delta T_p = T_6 - T_{2a} = 10.00$ K and increases at the hot end to $T_5 - T_3 = 94.15$ K. Because of the latter large temperature difference, the curvature of the cyclopentane isobar does not show any interference with the straight line of the heat carrier which can be cooled down to only 10 K above T_{2a} which is favorable for minimizing $\dot{C}_{HC}$. The temperature difference $T_5 - T_6$ is 228.86 K. On the other hand, the maximum cycle temperature T_3 is remarkably lower in the ORC-s2-system than in the TLC-system for Case I.

For the ORC-s2 -system in Case II the heat carrier line ranges from $T_6 = 428.68$ K to $T_5 = 553.15$ K with the upper pinch point temperature being $T_p = 510.06$ K, which is indicated in Fig. 5. The working fluid cyclopentane is heated from $T_{2a} = 384.29$ K to the temperature $T_3 = 529.00$ K. Hence, the temperature difference between the heat carrier and the working fluid amounts at the cold end to $T_6 - T_{2a} = 44.39$ K, decreases at the pinch point to $\Delta T_p = 10$ K and increases at the hot end to $T_5 - T_3 = 24.15$ K. Here, the temperature difference at the hot end is rather small and in order to keep the temperature difference between the straight line of the heat carrier and the strongly curved isobar of the working fluid larger or equal to $\Delta T_p = 10$ K the slope of the heat carrier line has to be rather flat. This results in the large temperature difference of 44 K at the cold end which is less favorable for minimizing $\dot{C}_{HC}$. The temperature difference $T_5 - T_6$ is only 124.47 K.

Fig. 6 shows the *T*, $\Delta\dot{H}$ -diagram for the heat transfer from the heat carrier to the working fluid cyclopentane in the ORC-o2 -systems for Case I and Case II. The dashed line refers to the heat carrier for Case I, the dashed-dotted line refers to the heat carrier for Case II. The full line shows the isobar of cyclopentane at the subcritical pressure $p_2 = 3.342$ MPa which reaches its boiling point at 489.00 K and continues horizontally till its dew point. One should note that this isobar shows a slight curvature before it reaches the boiling point.

For the ORC-o2 -system in Case I the heat carrier line ranges from $T_6 = 390.27$ K to $T_5 = 623.15$ K with the upper pinch point temperature being at the cold end, i.e. $T_p = T_6$, whilst the working fluid cyclopentane is heated from $T_{2a} = 380.27$ K to the temperature $T_3 = 489.00$ K. Hence, the temperature difference between the heat carrier and the working fluid amounts at the cold end with the pinch point $\Delta T_p = T_6 - T_{2a} = 10.00$ K and increases at the hot end to $T_5 - T_3 = 134.15$ K. Again, because of that large temperature difference, the curvature of the cyclopentane isobar does not show any interference with the straight line of the heat carrier which can be cooled down here in the o2 system like in the above considered s2 system to only 10 K above T_{2a} which is again favorable for minimizing $\dot{C}_{HC}$. The temperature difference $T_5 - T_6 = 232.88$ K is even 1.8% larger than for the Case I ORC-s2- system. On the other hand, the maximum cycle temperature T_3 is lower by 40 K in the ORC-o2-system than in the ORC-s2-system. As a consequence, η_{th} is larger by 7.5% for the s2-cycle than for the o2-cycle which can be seen from Table 10 of [24]. Hence, according to Eq. (18) the ORC-s2-system has a smaller $\dot{C}_{HC}$ value than the ORC-o2-system for Case I.

For the ORC-o2 -system in Case II the heat carrier line ranges from $T_6 = 408.70$ K to $T_5 = 553.15$ K. The pinch point which is indicated in Fig. 6 is somewhat below the boiling point with the upper pinch point temperature being $T_p = 483.47$. The working fluid cyclopentane is heated from $T_{2a} = 380.27$ K to the temperature $T_3 = 489.00$ K. Hence, the temperature difference between the heat carrier and the working fluid amounts at the cold end to $T_6 - T_{2a} = 28.43$ K, decreases at the pinch point to $\Delta T_p = 10$ K and increases at the hot end to $T_5 - T_3 = 64.15$ K. The present subcritical isobar does not interfere so much with the heat carrier straight line as the supercritical isobar which, as a consequence, allows a somewhat steeper slope of the heat carrier line. Hence the outlet temperature T_6 here is about 20 K lower than for the s2 case. This yields a temperature difference $T_5 - T_6$ for the o2 –cycle which is 16% larger than that for the s2- cycle. Even though η_{th} of the o2-cycle is smaller than that of the s2- cycle by 7% this can not balance the larger temperature difference and hence, according to Eq. (18), the o2 cycle has the smaller $\dot{C}_{HC}$ -value for Case II.

4. 2. Heat transfer from the working fluid

On the cold end one has a cooling agent with inlet temperature T_7 which may either be close to the environmental temperature or remarkably higher in case that the removed heat is still used as e.g. in district heating or a cascade process. The required mass flow $\dot{m}_{CA}$ of the cooling agent or its heat capacity flow rate $\dot{C}_{CA} = c_{p,CA} \cdot \dot{m}_{CA}$ will result from the design of the whole system.

4.2.1. Heat transfer from the working fluid in the TLC

In the TLC we have at state 4 wet vapour with temperature T_1 which has to be completely condensed by removing heat from the working fluid till it reaches state 1. The heat is transferred to the cooling agent which enters the system with temperature T_7 and leaves it with temperature T_8. The process is shown schematically in a T,h-diagram in Fig. 7 which also shows the pinch between points 4 and 8. The heat flow rate to be released by the working fluid is $\dot{Q}_{41} = \dot{m}_{WF}(h_1 - h_4)$ which is completely received by the cooling agent according to $\dot{Q}_{41} = -\dot{Q}_{78}$ The latter quantity can also be written as

$$\dot{Q}_{78} = \dot{C}_{CA}(T_8 - T_7). \tag{19}$$

As already mentioned we use throughout the paper $T_1 = T_7 + 23$ K. Moreover, we assume here as everywhere in this

paper that the temperature difference at the pinch point ΔT_p is 10 K, which means that $T_8 = T_1 - 10$ K. Hence, $T_8 - T_7 = 13$ K, which allows the calculation of the heat capacity flow rate $\dot{C}_{CA}$ of the cooling agent from Eq. (19).

4.2.2. Heat transfer from the working fluid in the ORC

In the ORC we have at state 4a superheated vapour with temperature T_{4a} which has firstly to be cooled down to state 1" which is the dew point corresponding to the boiling point state 1. There from the working fluid has to be completely condensed till it reaches state 1. The heat is transferred to the cooling agent which enters the system with temperature T_7 and leaves it with temperature T_8. The process is shown schematically in a T,h-diagram in Fig. 8 which also shows that there is a pinch between state 1" and a state of the cooling agent called 8a.

We make now similar assumptions for the temperatures as in Sec. 4.2.1. We prescribe the inlet temperature of the cooling agent T_7, assume for the condensation temperature of the working fluid $T_1 = T_7 + 23$ K and for the temperature difference at the pinch point $\Delta T_p = 10$ K, which means that $T_{8a} = T_1 - 10$ K or $T_{8a} - T_7 = 13$ K. In order to determine the heat capacity flow rate $\dot{C}_{CA}$ and the temperature T_8, we have to make now separate balances for the cooling and the condensation. Similarly as above, we have now for the condenser

$$|\dot{Q}_{1'',1}| = \dot{Q}_{7,8a} = \dot{C}_{CA}(T_{8a} - T_7), \tag{20}$$

wherefrom we obtain the heat capacity flow rate $\dot{C}_{CA}$. Next we have for the condenser

$$|\dot{Q}_{4a,1''}| = \dot{Q}_{8a,8} = \dot{C}_{CA}(T_8 - T_{8a}), \tag{21}$$

which allows the calculation of the temperature T_8.

4.3. Exergy equations

As we assume the cooling agent inlet temperature T_7 to be $T_7 = T_1 - 23$ K and the lowest value of T_1 in our case studies is 311.15 K, the lowest values for T_7 is 288.15 K (=15 °C) which we also assume to be the environmental temperature T_u.

Generally, for a state point i and a mass flow rate $\dot{m}$ the exergy flow rate $\dot{E}_i$ is given as

$$\dot{E}_i = \dot{m}_i e_i, \tag{22}$$

where e_i is the specific exergy at state i which is known to be

$$e_i = (h_i - h_u) - T_u(s_i - s_u), \tag{23}$$

where the subscript u refers to the conditions of the environment. If the flow of the fluid is isobaric and its heat capacity c_p is assumed as constant, we have

$$h_i - h_u = c_p(T_i - T_u), \tag{24}$$

$$s_i - s_u = c_p \ln(T_i/T_u), \tag{25}$$

and using the heat capacity flow rate $\dot{C} = \dot{m}c_p$ we obtain for the exergy flow rate

$$\dot{E}_i = \dot{C}[(T_i - T_u) - T_u \ln(T_i/T_u)]. \tag{26}$$

The latter equation can now be specified for the incoming exergy flow rate $\dot{E}_5$ and the outgoing exergy flow rate $\dot{E}_6$ of the heat carrier as well as for the incoming exergy flow rate $\dot{E}_7$ and the outgoing exergy flow rate $\dot{E}_8$ of the cooling agent by using for T_i the appropriate temperatures.

With Eq. (26) the exergy efficiencies defined in the Introduction can now be formulated. The exergy efficiency for power production ξ_p was defined as ratio of the net power output to the incoming exergy flow rate of the heat carrier and is obtained as

$$\xi_P = |\dot{W}|/\{\dot{C}_{HC}[(T_5 - T_u) - T_u \ln(T_5/T_u)]\}, \tag{27}$$

whilst the total exergy efficiency ξ defined as ratio of all outgoing exergy flows to all incoming exergy flows is given as

$$\xi = (|\dot{W}| + \dot{E}_6 + \dot{E}_8)/(\dot{E}_5 + \dot{E}_7). \tag{28}$$

5. Case studies

In this Section we consider five cases which are characterized by different pairs of inlet temperatures of the heat carrier T_5 and of the cooling agent T_7. General assumptions throughout are, that $T_1 = T_7 + 23$ K and that all pinch point temperature differences ΔT amount to 10 K. This refers to the pinch points in the heater, in the condenser or the cooler-condenser and for the ORC in the IHE ($T_{4a} = T_2 + 10$ K). Next, we assume for the isentropic pump efficiency $\eta_{sP} = 0.65$ and for the isentropic expander efficiency $\eta_{sE} = 0.85$. Finally, all flow rates will be given for a net power output $|\dot{W}|$ of 1 MW.

The thermodynamic data for water are taken from the Wagner equation of state [46] which is easily accessible via the NIST webbook [47]. For the organic working fluids we use the BACKONE equation of state [48] with the substance specific parameters given in [24,49].

In the following subsections we will discuss details of the particular cases. The data for all cases are summarized in Table 1. First, this table shows the heat carrier inlet temperature T_5 and the cooling agent inlet temperature T_7. Then the table shows the optimal cycle type and working fluid followed by the optimal case results for the cycle data T_1, T_{2a}, T_3, T_4, T_{4a}, p_1, p_3, $\dot{V}_3$, $\dot{V}_4$, $\dot{Q}_{2,2a}$, x, η_{th}, for the heat carrier data T_6, T_p, $|\dot{Q}_{56}|$, $\dot{C}_{HC}$, and for the cooling agent data T_8, $\dot{Q}_{78}$, $\dot{C}_{CA}$. Finally, the optimal case results for the exergies $\dot{E}_5$, $\dot{E}_6$, $\dot{E}_7$, $\dot{E}_8$ and for the exergy efficiencies ξ and ξ_p are shown.

5.1. Case I: $T_5 = 350$ °C, $T_7 = 62$ °C

The Case I input data are $T_5 = 623.15$ K, $T_7 = 333.15$ K, and consequently $T_1 = 358.15$ K.

For the TLC the only free parameter is the boiling temperature T_3. Using the optimization criterion of minimal heat capacity flow rate $\dot{C}_{HC}$ of the heat carrier for net power production $|\dot{W}| = 1$MW we found by trial and error as optimal value $T_3 = 590$ K. For that temperature the heat capacity flow rate $\dot{C}_{HC}$ being the objective function is $\dot{C}_{HC} = 20.00$kW/K , the exergy efficiency for power production is $\xi_p = 0.44$, and the total exergy efficiency is $\xi = 0.87$. For all the other data we refer to Table 1.

For the ORC we have found in [24] that the lowest value of $\dot{C}_{HC}$ is obtained with cyclopentane in the supercritical s2 cycle. The pressure p_3 was taken to be $1.2p_c$ with p_c being the critical pressure as the value $1.2p_c$ was found in [24] to be an optimal pressure for supercritical cycles. The temperature $T_3 = 529$ K was determined by the consideration that 1) higher temperatures on the selected isobar increase $\dot{C}_{HC}$ and that 2) the expansion should not go through the wet vapour region. Hence the criterion for T_3 is that the entropy at state point 3 on the isobar $p = 1.2p_c$ is just slightly larger than the maximum entropy on then dew line which occurs at 489 K. For that optimized point 3 one obtains for the heat capacity flow rate $\dot{C}_{HC} = 23.45$kW/K, for the exergy efficiency for power production $\xi_p = 0.38$, and for the total exergy efficiency $\xi = 0.84$. For all the other data we refer again to Table 1. We mention that we

Table 1
Results for minimal heat capacity flow rate $\dot{C}_{HC}$ of the heat carrier at given heat carrier inlet temperature $T_{in,HC} = T_5$, cooling agent inlet temperature $T_{in,CA} = T_7$, and net power output $|\dot{W}| = 1$ MW ($T_1 = T_7 + 23$ K, $T_u = 288.15$ K, pinch point temperature differences $\Delta T = 10$ K, $\eta_{sP} = 0.65$, $\eta_{sT} = 0.85$).

	Case I		Case II		Case III		Case IV		Case V	
T_5 (K)	623.15		553.15		553.15		493.15		423.15	
T_7 (K)	335.15		335.15		288.15		288.15		288.15	
Cycle type	TLC	ORC-s2	TLC	ORC-o2	TLC	ORC-o2	TLC	ORC-s2	TLC	ORC-s2
Work fluid	water	cC_5H_{10}	water	cC_5H_{10}	water	cC_5H_{10}	water	nC_4H_{10}	water	C_3H_8
T_1 (K)	358.15	358.15	358.15	358.15	311.15	311.15	311.15	311.15	311.15	311.15
T_{2a} (K)	–	384.29	–	380.27	–	337.65	–	321.54	–	–
T_3 (K)	590.00	529.00	534.00	489.00	534.00	470.00	479.00	443.60	412.00	390.00
T_4 (K)	358.15	401.00	358.15	396.41	311.15	357.09	311.15	333.55	311.15	314.03
T_{4a} (K)	–	372.88	–	370.63	–	322.96	–	324.86	–	–
p_1 (kPa)	57.87	288.8	57.87	288.8	6.633	68.88	6.633	359.7	6.633	1309
p_3 (kPa)	10,821	5412	4757	3342	4757	2546	1754	4706	350	5097
$\dot{V}_3$(l/s)	7.00	51.0	10.4	121.0	6.24	113.7	9.53	74.8	22.4	201.3
$\dot{V}_4$(l/s)	4993	1778	6540	1937	33,546	4824	43,550	1711	69,896	997
$\dot{Q}_{2,2a}$(kW)	–	539	–	530	–	380	–	236	–	–
x	0.3739	–	0.2843	–	0.3184	–	0.2466	–	0.1561	–
η_{th}	0.1979	0.1863	0.1585	0.1727	0.2183	0.2329	0.1706	0.1608	0.1136	0.1024
T_6 (K)	370.53	394.29	369.15	408.70	322.39	372.89	321.42	333.18	321.22	335.48
T_p (K)	416.16	394.29	386.57	483.47	388.53	480.00	321.42	368.16	321.22	370.32
$\lvert\dot{Q}_{56}\rvert$(kW)	5054	5368	6309	5790	4581	4294	5862	6217	8800	9766
$\dot{C}_{HC}$(kW/K)	20.00	23.45	34.29	40.08	19.85	23.82	34.14	38.86	86.33	111.4
T_8 (K)	348.15	348,94	348.15	348,85	301.15	301.65	301.15	302.13	301.15	301.42
$\dot{Q}_{78}$(kW)	4054	4368	5308	4790	3746	3309	4862	5217	7800	8766
$\dot{C}_{CA}$(kW/K)	311.81	316.63	408.30	349.66	288.15	245.15	374.00	373.2	600.0	660.6
$\dot{E}_5$(kW)	2255	2644	2643	3016	1530	1836	1713	1950	2096	2705
$\dot{E}_6$(kW)	198	370	330	795	37	249	61	124	152	391
$\dot{E}_7$(kW)	1080	1096	1413	1210	0	0	0	0	0	0
$\dot{E}_8$(kW)	1714	1784	2244	1964	82	75	106	99	171	196
ξ	0.8732	0.8440	0.8812	0.8895	0.7314	0.7211	0.6813	0.6272	0.6312	0.5867
ξ_p	0.4435	0.3782	0.3784	0.3316	0.6536	0.5447	0.5838	0.5128	0.4771	0.3697

have investigated in [24] also a) the o2 cycle with $T_3 = 489$ K and $p_3 = 0.74p_c$ where the maximal entropy on the dew line occurs and b) the o3 cycle with $p = 0.9p_c$ and $T_3 = 513.45$ K which is 10 K higher than the saturation temperature for $p = 0.9p_c$ in order to avoid expansion through the wet region. We found for the o2 cycle $\dot{C}_{HC} = 24.9$kW/K ($\xi_p = 0.36$) and for the o3 cycle $\dot{C}_{HC} = 24.0$kW/K ($\xi_p = 0.37$) which are both slightly worse than for the s2 cycle.

Comparing the optimized results for the TLC and the ORC-s2 cycle we note that the exergy efficiency for power production ξ_p is larger by 17% for the TLC. The better ξ_p result of the TLC in comparison with the ORC-s2 is caused by the difference in the heat transfer to the working fluid shown in Figs. 4 and 5 which was discussed in Sec. 4.2. The difference in the heat transfer between the ORC- s2 and the ORC-o2 can be seen from Figs. 5 and 6 and was also discussed in Sec. 4.2.

It is also seen from Table 1 that the total exergy efficiency ξ is only larger by 3% for the TLC than for the ORC-s2. The main reason for that small difference is that the outlet temperature T_6 of the heat carrier is 24 K higher for the ORC than for the TLC and hence also the outgoing exergy flow rate of the heat carrier $\dot{E}_6$ is remarkably higher for the ORC which is favorable for cascade systems or in CHP plants.

Finally, we want to draw the attention to the volume flows at the inlet of the expander $\dot{V}_3$ and at the outlet of the expander $\dot{V}_4$. For the TLC the volume flow $\dot{V}_3$ is 7.00 l/s and increases up to $\dot{V}_4 = 4993$ l/s which is an increase by a factor of 710. For the ORC the volume flow $\dot{V}_3$ is 51.0 l/s and increases up to $\dot{V}4 = 1778$ l/s which is an increase by a factor of 35.

5.2. Case II: $T_5 = 280$ °C, $T_7 = 62$ °C

The Case II input data are $T_5 = 553.15$ K, $T_7 = 333.15$ K, and consequently $T_1 = 358.15$ K.

For the TLC we found by trial and error as optimal temperature $T_3 = 534$ K. For that temperature the heat capacity flow rate is $\dot{C}_{HC} = 34.29$kW/K, the exergy efficiency for power production is $\xi_p = 0.38$, and the total exergy efficiency is $\xi = 0.88$.

For the ORC we have found in [24] that the lowest value of $\dot{C}_{HC}$ is obtained with cyclopentane in the subcritical o2 cycle. with $T_3 = 489$ K and $p_3 = 0.74p_c$ where the maximal entropy on the dew line occurs. For that optimized point 3 one obtains for the heat capacity flow rate $\dot{C}_{HC} = 40.08$kW/K , for the exergy efficiency for power production $\xi_p = 0.33$, and for the total exergy efficiency $\xi = 0.89$. We mention that we have investigated in [24] also the s2 and the o3 cycle with the same state points 3 as in Case I. We found for the s2 cycle $\dot{C}_{HC} = 43.1$kW/K ($\xi_p = 0.30$) and for the o3 cycle $\dot{C}_{HC} = 44.6$kW/K ($\xi_p = 0.29$) which are both somewhat worse than for the o2 cycle. It is interesting to note that in Case I the best ORC cycle is of s2 type whilst in Case II the best ORC cycle is o2. This difference is again caused by the heat transfer as is shown in Figs. 5 and 6 and was discussed in Sec. 4.2.

Comparing the optimized results for the TLC and the ORC-o2 cycle we note that the exergy efficiency for power production ξ_p is larger by 14% for the TLC. On the other hand, the total exergy efficiency ξ is now even slightly larger for the ORC than for the TLC which is caused by the rather high outlet temperature of the heat carrier T_6.

Finally, we note that the volume flows show a similar behavior is in Case I.

5.3. Case III: $T_5 = 280$ °C, $T_7 = 15$ °C

The Case III input data are $T_5 = 553.15$ K, $T_7 = 288.15$ K, and consequently $T_1 = 311.15$ K.

For the TLC we have as in Case II as optimal temperature $T_3 = 534$ K. Then the heat capacity flow rate is $\dot{C}_{HC} = 19.85$kW/K,

the exergy efficiency for power production is $\xi_p = 0.65$, and the total exergy efficiency is $\xi = 0.73$.

The best ORC was found with cyclopentane in an o2 cycle with $T_3 = 470$ K and $p/p_c = 0.5645$. Therewith, $\dot{C}_{HC} = 23.82$kW/K, $\xi_p = 0.54$, and $\xi = 0.72$.

Comparing the optimized results for the TLC and the ORC-o2 cycle we note that the exergy efficiency for power production ξ_p is larger by 20% for the TLC whilst the total exergy efficiency ξ is only larger by 1.4% for the TLC than for the ORC-o2. These results can be understood first by the very good match of the heat carrier and the working fluid curves for the TLC in the T,$\Delta\dot{H}$ -diagram shown in Fig. 4. Second, for the ORC-o2 cycle the pinch occurs at the boiling point and the heat carrier outlet temperature T_6 is 35 K higher than the temperature T_{2a} of the working fluid at the inlet of the heater.

Finally, we note that the volume flows at the inlet of the expander $\dot{V}_3$ are of the same order as in Cases I and II. At the outlet of the expander $\dot{V}_4$, however, becomes very high in particular for the TLC where it amounts to 33,546 l/s. The reason for that is low water vapour pressure of 6.6 kPa at the outlet temperature 311.15 K.

5.4. Case IV: $T_5 = 220$ °C, $T_7 = 15$ °C

The Case IV input data are $T_5 = 493.15$ K, $T_7 = 288.15$ K, and consequently $T_1 = 311.15$ K.

For the TLC we have found now as optimal temperature $T_3 = 479$ K. Then the heat capacity flow rate is $\dot{C}_{HC} = 34.14$kW/K, the exergy efficiency for power production is $\xi_p = 0.58$, and the total exergy efficiency is $\xi = 0.68$.

For the ORC we did not consider cyclopentane anymore as working fluid because its critical temperature $T_c = 511.7$ K is too high for the given value of $T_5 = 493.15$ K. Instead, we considered n-pentane with $T_c = 469.65$ K and n-butane with $T_c = 425.20$ K. For n-pentane we performed calculations for o2-cycles and found the minimal heat capacity flow rate $\dot{C}_{HC}$ for $T_3 = 413.43$ K as $\dot{C}_{HC} = 43.55$kW/K For n-butane we considered an s2-cycle with $p_3 = 1.2p_c$ and $T_3 = 443.60$ K. The criterion for selection of T_3 is the same as in Case I, namely that the entropy at state point 3 on the isobar $p = 1.2p_c$ is just slightly larger than the maximum entropy on the dew line. With this selection we obtained for n-butane $\dot{C}_{HC} = 38.86$ which is 11% lower than the optimal o2 result with n-pentane. Furthermore, this ORC-s2 cycle with n-butane yields for the exergy efficiency for power production $\xi_p = 0.51$ and for the total exergy efficiency $\xi = 0.63$.

Comparing the optimized results for the TLC and the ORC-s2 cycle we note that the exergy efficiency for power production ξ_p is larger by 14% for the TLC whilst the total exergy efficiency ξ is larger by 9% for the TLC than for the ORC-s2. These results agree quite well with those obtained in the previous cases.

Regarding the volume flows, the $\dot{V}_4$ value for the TLC becomes now still higher as in Case III because for the same net power output $|\dot{W}| = 1$MW and a lower value of T_5 the water mass flow has to increase. For the organic working fluid the value $\dot{V}_4$ decreases in going from cyclopentane for Case III to n-butane in Case IV because the vapour pressure of n-butane is five times larger than that of cyclopentane at $T_1 = 311.15$ K.

5.5. Case V: $T_5 = 150$ °C, $T_7 = 15$ °C

The Case V input data are $T_5 = 423.15$ K, $T_7 = 288.15$ K, and consequently $T_1 = 311.15$ K.

For the TLC we have found now as optimal temperature $T_3 = 412$ K. Then the heat capacity flow rate is $\dot{C}_{HC} = 86.33$kW/K, the exergy efficiency for power production is $\xi_p = 0.48$, and the total exergy efficiency is $\xi = 0.63$.

For the ORC we take now propane as working fluid. This choice is based on the idea to have a similar ratio T_c/T_5 as in Case IV where this ratio is 0.86. In Case V the heat carrier inlet temperature is 423.15 K and with the critical temperature of propane being $T_c = 369.825$ K one obtains the ratio $T_c/T_5 = 0.87$. Before discussing the results we want to mention two peculiarities of this case.

First, the coexistence curve of propane in the T,s-diagram is bell-shaped in contrary to cyclopentane and n-butane, which have an overhanging dew line. This simply is a consequence of our hypothesis [24] that the coexistence curve in the T,s-diagram becomes less skewed with decreasing ideal gas heat capacity of the considered fluid.

The second peculiarity is a consequence of the first. As the dew line is not overhanging the end point 4 of a dry expansion in the turbine does not need to be far away from the dew line and in such a case an IHE is not required.

We decided to consider again an ORC-s2 cycle with the supercritical isobar for $p_3 = 1.2p_c$ and took $T_3 = 390$ K. This selection of point 3 resulted in a temperature $T_4 = 314.03$ K which is between $T_1 = 311.15$ K and $T_2 = 315.81$ K. With this point 3 we obtain for the heat capacity flow rate $\dot{C}_{HC} = 111.4$kW/K, for the exergy efficiency for power production $\xi_p = 0.37$, and for the total exergy efficiency $\xi = 0.59$.

Comparing the optimized results for the TLC and the ORC-s2 cycle we note that the exergy efficiency for power production ξ_p is now larger by 29% for the TLC whilst the total exergy efficiency ξ is larger by 8% for the TLC than for the ORC-s2.

We were somewhat surprised about this 29% higher TLC result because in Cases I to IV ξ_p for TLC was only higher than for ORC by 14%–20%. Hence, we checked our calculation by using alternatively to BACKONE the NIST webbook [47] which is based on the reference equations [50,51]. Taking the same point 3 as above we obtained now for $\xi_p = 0.3547$ which is even 4% lower than the BACKONE result. We learn two things from this check. First, the BACKONE results are even for supercritical pressures sufficiently accurate. Second, whilst the TLC results for ξ_p decrease roughly linearly from Case III to V, the ORC results decrease stronger with decreasing heat carrier inlet temperature. The latter finding, however, leaves some room for speculation. The TLC results are considered inherently as being more consistent than the ORC results because always the same working fluid is taken and only the maximum cycle temperature T_3 is varied. In the ORC, however, not only the pressure p_3 and the temperature T_3 are varied but also the working fluid. The crucial point with pure working fluids, however, is that their thermodynamic properties do not vary continuously in going from one substance to another.

Finally, looking on the volume flows we see that the ORC-s2 values are $\dot{V}_3 = 201$ l/s and $\dot{V}_4 = 997$ l/s, whilst TLC values increase from $\dot{V}_3 = 22$ l/s to $\dot{V}_4 = 69,896$ l/s.

6. Comparison with literature results

The remaining task is an explanation for the remarkable difference between our findings on the one hand and the estimates of Löffler [40] and the results of Zamfirescu and Dincer [43] on the other hand.

The estimate of Löffler is based on his Figs. 2 and 3 in Ref. [40]. In Fig. 2 he compares a TLC and an ORC in a T,s-diagram and in Fig. 3 he approximates the ORC by a Carnot cycle. The difference between that assumption and our calculations can be seen from Figs. 2 and 4 in [24] which show schematically the T,s-diagram of a subcritical high-pressure ORC and a supercritical ORC. Moreover, the present Figs. 5 and 6 show quantitatively that for these high pressure cycles the heat carrier and the working fluid curves in the heater do not

match so bad in the T, $\Delta\dot{H}$ − diagram as one may conjecture from the Figs in Ref. [40].

Regarding now the results of Zamfirescu and Dincer [43] we want to mention that their quantity ε_{so} is just our exergy efficiency for power production ξ_p. In their Table 3 they present results for ξ_p ($=\varepsilon_{so}$) for ORC, Kalina and TLC cycles.

For the ORC, Zamfirescu and Dincer [43] selected as working fluids the substances 141b (CHCl2-CH2F, $T_c = 477.5$ K, o-fluid), R123 (CF3-CHCl2, $T_c = 456.83$ K, o-fluid), R245ca (CF3-CHF2, $T_c = 447.57$ K, o-fluid) and R21 (CF2Cl2, $T_c = 451.48$ K, b-fluid). Following [11] we use the notations "b-" for fluids with bell-shaped and "'o-'' for fluids with overhanging saturation line. In [43] the best ξ_p result was obtained for the b-fluid R21 as $\xi_p = 0.21$ using the boundary conditions $T_5 = 423.15$ K (150 °C), $T_7 = 298.15$ K (25 °C), and $T_1 = 313.15$ K (40 °C) as well as $T_u = 298.15$ K (25 °C) and $\eta_{s,P} = 0.70$. Moreover, one observes from [43] that for the o-fluids the ξ_p results become better with decreasing critical temperature. Hence, our hypothesis is that the substances selected in [43] have too high critical temperatures and hence too low pressures for their boundary conditions (For R21 $p_3 = 0.28p_c$). In order to check our hypothesis we simply made a test calculation with n-butane ($T_c = 425.125$ K, o-fluid) using the same boundary conditions as in [43] and the NIST-webbook [47] based on the reference equations [51,52]. For an ORC-o2 without IHE and the frequently used, non optimized pressure $p_3 = 2.0$ MPa ($T_3 = 387.52$ K) we obtained $\xi_p = 0.24$ which is already 20% higher than the best value $\xi_p = 0.20$ for an overhanging working fluid (R245ca) considered in [43]. That pressure p_3, however, is still only $0.53p_c$ whilst in our case V which uses similar boundary conditions as [43] the supercritical propane ORC with $p_3 = 1.2p_c$ yields $\xi_p = 0.37$.

We also performed a TLC calculation with water for the same boundary conditions as in [43]. using again the Wagner equation [46,47]. We found as optimal temperature $T_3 = 412$ K and therefrom $\xi_p = 0.45$ which has to be compared with a value $\xi_p = 0.43$ for an ammonia + water mixture given in [43]. Whilst the agreement is acceptable taking into account some power loss for the air fan considered in [43] the result, however, raises the question why it is advantageous to use an ammonia + water mixture instead of pure water as working fluid. A little advantage might be the temperature glide of the mixture in the condenser. The big disadvantage, however, is the corrosive behavior of ammonia which requires expensive material for the plant.

7. Summary and conclusions

For comparison of ORC and TLC we have performed optimized case studies for five pairs of heat carrier inlet temperatures T_5 and cooling agent inlet temperatures T_7 being (350 °C, 62 °C), (280 °C, 62 °C), (280 °C, 15 °C), (220 °C, 15 °C) and (150 °C, 15 °C). The working fluid for TLC was water. For the ORC the working fluid was cyclopentane for $T_5 = 350$ °C and 280 °C, n-butane for $T_5 = 220$ °C and propane for $T_5 = 150$ °C and optimal results were obtained with slightly sub- or supercritical pressures.

We found that the exergy efficiency for power production ξ_p which is the ratio of the net power output to the incoming exergy flow of the heat carrier is higher for the TLC than for the ORC between 14% and 20% for T_5 from 350 °C to 220 °C. For $T_5 = 150$ °C the exergy efficiency for power production ξ_p is higher for the TLC by 29%. The total exergy efficiency ξ which is the ratio of all outgoing exergy flows to all incoming exergy flows is slightly larger for the ORC than for the TLC for the case (280 °C, 62 °C), in the other cases TLC is better between 1% and 9%. For a change of T_5 the exergy efficiencies of ORC do not change in a systematic way as optimal results are obtained from different organic working fluids and/or different cycle types.

Other quantities of interest are the volume flow rates $\dot{V}_3$ at the inlet and $\dot{V}_4$ at the outlet of the expander which are important for the design of the expander and also for the sizing of the heat exchangers. The outgoing volume flows $\dot{V}_4$ from the expander are larger for the TLC than for the ORC by a factor of 2.8 for case I with the minimum working fluid temperature $T_1 = 85$ °C and by a factor of 70 for case V with $T_1 = 38$ °C. The ratios $\dot{V}_4/\dot{V}_3$ are for the ORC between 5 and 42, but amount for the TLC 710 and 630 for the cases I and II with $T_1 = 85$ °C and even between 5400 and 3100 for the cases III to V with $T_1 = 38$ °C. These large volume flows $\dot{V}_4$ for TLC with water as working fluid for lower T_1 may be difficult to handle in real plants. Hence, the application of TLC with water as working fluid is mainly recommended for higher values of the minimum working fluid temperature T_1 or higher values of the cooling agent inlet temperature T_7. Examples are combined heat power plants or upper stages in cascade heat to power conversion systems. An advantage of water as working fluid in comparison with organic substances is its non-flammability.

The large volume flows $\dot{V}_4$ for TLC with water as working fluid for lower T_1 is caused by the low water vapour pressures at lower temperatures; at $T_1 = 38$ °C, e.g. the vapour pressure of water is only $p_s = 6.633$ kPa. Hence the volume flows $\dot{V}_4$ in TLC can be decreased by using working fluids with higher vapour pressures. Examples could be cyclopentane ($T_c = 511.7$ K, $p_s = 68.88$ kPa), n-pentane ($T_c = 469.65$ K, $p_s = 109.2$ kPa), n-butane ($T_c = 425.20$ K $p_s = 359.7$ kPa), propane ($T_c = 369.825$ K, $p_s = 1309$ kPa) or a refrigerant like HFO-1234yf ($T_c = 367.85$ K, $p_s = 971.6$ kPa). The critical temperatures T_c are an upper limit for the use of these substances in TLC and the vapour pressures p_s are given as demonstration examples at 38 °C and were obtained from BACK-ONE [24,49,53]. The mentioned organic substances have auto-ignition temperatures which are higher than their critical temperatures and have low global warming potentials.

An additional improvement of TLC and ORC can be obtained by using mixtures [54] as working fluids because of their temperature glide in the condenser which yields a better match to the cooling agent in the T,h-diagram.

Acknowledgments

This work was motivated by presentations of Dr. Michael Löffler from the European Institute for Energy Research (EIFER), Karlsruhe, at the Thermodynamik –Kolloquia in Berlin (2009) and Bayreuth (2010). In particular, the author thanks Dr. Löffler for sending him Ref. [44] prior to publication. Moreover, the author acknowledges gratefully the help of Johannes Arnberger and of Verena Wetter for their technical support in the preparation of this paper.

References

[1] Carnot S. Reflexions sur la puissance motrice du feu et sur les machines propres a developper cette puissance. Paris, 1824. Reprinted in Annales scientifiques de l'Ecole normale superieure 1872; 2.ser., t.1 (in French).
[2] Clausius R. Über die Anwendung der mechanischen Wärmetheorie auf die Dampfmaschine. Ann Phys Chem 1854;173:441–76. 513–558 (in German).
[3] Rankine WJM. Miscellaneous scientific papers. London: Charles Griffin and Company, http://www.archive.org/details/miscellaneousscii00rank; 1881.
[4] Rogers G, Mayhew Y. Engineering thermodynamics, work and heat transfer. 4th ed. Harlow: Longman Scientific & Technical; 1992 (pp. 239–243).
[5] ORC-HP-technology. In: VDI- Berichte 539. VDI–Verlag Düsseldorf, ISBN 3180905395; 1984. Proceedings of VDI-Seminar 10–12 Sept. 1984 ETH Zürich.
[6] Hammer H, Röhmfeld M. Abwärmenutzung zur Krafterzeugung mittels neuer Kreislaufmedien. In: VDI-Bericht 415. VDI-Verlag Düsseldorf; 1981. p. 81–7 (in German).
[7] Larjola J. Electricity from industrial heat using high-speed organic Rankine cycle (ORC). Int J Prod Econom 1995;41:227–35.
[8] Angelino G, Colonna P. Organic Rankine cycles for energy recovery from molten carbonate fuel cells. In 35th Intersociety Energy Conversion Engineering Conference and Exhibit. Las Vegas, NV. Reston, VA: AIAA; 2000.

[9] Angelino G, Colonna P. Air cooled siloxane bottoming cycle for molten carbonate fuel cells. In: 2000 Fuel Cell Seminar, No 114, Portland, OR; 2000.
[10] Obernberger I, Hammerschmid A, Bini R. Biomasse-Kraft-Wärme-Kopplungen auf Basis des ORC-Prozesses-EU-THERMIE-Projekt Admont (A). In: Proc. VDI-Tagung Thermische Nutzung von fester Biomasse, Salzburg, Mai 2001. VDI Bericht 1588. VDI-Verlag Düsseldorf, ISBN 3-18-091588-9; 2001. p. 283–302 (in German).
[11] Saleh B, Koglbauer G, Wendland M, Fischer J. Working fluids for low-temperature organic Rankine cycles. Energy 2007;32:1210–21.
[12] Hettiarachchia HDM, Golubovica M, Worek WM, Ikegami Y. Optimum design criteria for an organic Rankine cycle using low-temperature geothermal heat sources. Energy 2007;32:1698–706.
[13] Wei DH, Lu XS, Lu Z, Gu J. Performance analysis and optimization of organic Rankine cycle (ORC) for waste heat recovery. Energy Conversion Manage 2007;48:1113–9.
[14] Drescher U, Brueggemann D. Fluid selection for the organic Rankine cycle (ORC) in biomass power and heat plants. Appl Therm Eng 2007;27:223–8.
[15] Desai NB, Bandyopadhyay S. Process integration of organic Rankine cycle. Energy 2009;34:1674–86.
[16] Schuster A, Karellas S, Kakaras E, Spliethoff H. Energetic and economic investigation of organic Rankine cycle applications. Appl Therm Eng 2009;29: 1809–17.
[17] Kosmadakis G, Manolakos D, Kyritsis S, Papadakis G. Comparative thermo-dynamic study of refrigerants to select the best for use in the high-temperature stage of a two-stage organic Rankine cycle for RO desalination. Desalination 2009;243:74–94.
[18] Dai YP, Wang JF, Gao L. Parametric optimization and comparative study of organic Rankine cycle (ORC) for low grade waste heat recovery. Energy Convers Manage 2009;50:576–82.
[19] Wang XD, Zhao L. Analysis of zeotropic mixtures used in low-temperature solar Rankine cycles for power generation. Solar Energy 2009;83:605–13.
[20] Chacartegui R, Sanchez D, Munoz JM, Sanchez T. Alternative ORC bottoming cycles for combined cycle power plants. Appl Energy 2009;86:2162–70.
[21] Yari M. Exergetic analysis of various types of geothermal power plants. Renew Energy 2010;35:112–21.
[22] Tchanche BF, Papadakis G, Lambrinos G, Frangoudakis A. Fluid selection for a low-temperature solar organic Rankine cycle. Appl Therm Eng 2009;29: 2468–76.
[23] Lakew AA, Bolland O. Working fluids for low-temperature heat source. Appl Therm Eng 2010;30:1262–8.
[24] Lai NA, Wendland M, Fischer J. Working fluids for high-temperature organic Rankine cycles. Energy 2011;36:199–211.
[25] Gang Pei, Jing Li, Yunzhu Li, Dongyue Wang, Jie Ji. . Construction and dynamic test of a small-scale organic Rankine cycle. Energy 2011;36:3215–23.
[26] Guo T, Wang HX, Zhang SJ. Fluids and parameters optimization for a novel cogeneration system driven by low temperature geothermal sources. Energy 2011;36:2639–49.
[27] Sauret E, Rowlands AS. Candidate radial-inflow turbines and high-density working fluids for geothermal power systems. Energy 2011;36:4460–7.
[28] DiPippo R. Second law assessment of binary plants generating power from low - temperature geothermal fluids. Geothermics 2004;33:565–86.
[29] Wang J, Dai Y, Gao L. Exergy analyses and parametric optimizations for different cogeneration power plants in cement industry. Appl Energy 2009; 86:941–8.
[30] Bombarda P, Ivernizzi CM, Pietra C. Heat recovery from Diesel engines: a thermo-dynamic comparison between Kalina and ORC cycles. Appl Therm Eng 2010;30:212–9.
[31] Kalina AI. Combined-cycle system with novel bottoming cycle. J Eng for Gas Turbines Power – Trans ASME 1984;106:737–42.
[32] Wall G, Chuang CC, Ishida M. Exergy study of the Kalina cycle. Advanced Energy Systems. In: Bajura RA, von Spakovsky MR, Geskin ES, editors. Analysis and Design of Energy Systems: Analysis of Industrial Processes, vol. 10-3. ASME. p. 73–7, http://exergy.se/ftp/kalina.pdf; 1989.
[33] Park YM, Sonntag RE. A preliminary study of the Kalina power cycle in connection with a combined cycle system. Int J Energy Res 1990;14:153–62.
[34] Marston CH. Parametric analysis of the Kalina cycle. J Eng for Gas Turbines Power – Trans ASME 1990;112:107–16.
[35] Heppenstall T. Advanced gas turbine cycles for power generation: a critical review. Appl Therm Eng 1998;18:837–46.
[36] Hettiarachchi HDM, Golubovic M, Worek WM, Ikegami Y. The performance of the Kalina cycle system 11 (KSC–11) with low-temperature heat sources. J Energy Resour Technol – Transactions ASME 2007;129:243–7.
[37] Smith IK. Matching and work ratio in elementary thermal power plant theory; Proceedings of the Institution of Mechanical Engineers, Part A. J Power Energy 1992;206:257–62.
[38] Crook AW. Profiting from low-grade heat. The Watt Committee on Energy. Report No. 26. Institution of Electrical Engineers; 1994. ISBN-10:0852968353, ISBN-13: 978–0852968352.
[39] Kliem BP. Grundlagen des Zweiphasen-Schraubenmotors – Fundamentals of the Two-Phase Screw-Type Engine, Dissertation, Fakultät für Maschinenbau, Universität Dortmund, 2005 (in German).
[40] Löffler M. Kreisprozess mit Flashverdampfung im Arbeitsraum einer Kolbenmaschine. VGB PowerTech. Int J for Electricity Heat Generation 2007;7:92–7 (in German).
[41] DiPippo R. Ideal thermal efficiency for geothermal binary plants. Geothermics 2007;36:276–85.
[42] Löffler M. Flash evaporation in Cyclones. Chem Eng Technol 2008;31:1062–5.
[43] Zamfirescu C, Dincer I. Thermodynamic analysis of a novel ammonia–water trilateral Rankine cycle. Thermochimica Acta 2008;447:7–15.
[44] Löffler M, Steffen M, Schaber K. Umsetzung einer Kolbendampfmaschine mit interner Flashverdampfung, Abschlussbericht über ein Entwicklungsprojekt, gefördert unter dem Az: 25116 – 21/0 von der Deutschen Bundesstiftung Umwelt (DBU), Oktober 2010 (in German).
[45] Koglbauer G, Saleh B, Wendland M, Fischer J. Arbeitsmedien für Niedrigtemperatur-ORC-Prozesse, Proc. 9. Symposium Energie innovation, 15. - 17 Februar 2006, TU Graz, Verlag der TU Graz, ISBN 3-902465-30-1, Graz 2006.pp 170 –1. (in German)
[46] Wagner W, Pruss A. The IAPWS formulation 1995 for the thermodynamic properties of ordinary water substance for general and scientific use. J Phys Chem Ref Data 2002;31:387–535.
[47] NIST Chemistry WebBook, Thermophysical properties of fluids, http://webbook.nist.gov/chemistry/fluid/.
[48] Müller A, Winkelmann J, Fischer J. The Backone family of equations of state: 1. Nonpolar and polar pure fluids. AIChE J 1996;42:1116–26.
[49] Wendland M, Saleh B, Fischer J. Accurate thermodynamic properties from the BACKONE equation for the processing of natural gas. Energy Fuels 2004;18: 938–51.
[50] Miyamoto H, Watanabe K. A thermodynamic property model for fluid-phase propane. Int J Thermophys 2000;21:1045–72.
[51] Younglove BA, Ely JF. Thermophysical properties of fluids. II. Methane, ethane, propane, isobutane and normal butane. J Phys Chem Ref Data 1987;16:577–798.
[52] Miyamoto H, Watanabe K. A thermodynamic property model for fluid-phase n-butane. Int J Thermophys 2001;22:459–75.
[53] Lai NA, Vrabec J, Raabe G, Fischer J, Wendland M. Description of HFO-1234yf with BACKONE equation of state. Fluid Phase Equilibria 2011;305:204–11.
[54] Weingerl U, Wendland M, Fischer J, Müller A, Winkelmann J. Backone family of equations of state: 2. Nonpolar and polar fluid mixtures. AIChE J 2001;47: 705–17.